Modeling of micro-perforated panels in a complex vibro-acoustic environment using patch transfer function approach

L. Maxit

Laboratoire Vibrations-Acoustique, INSA Lyon, 25 bis, av. Jean Capelle, 69621 Villeurbanne Cedex, France

C. Yang and L. Cheng[a]

Department of Mechanical Engineering, The Hong Kong Polytechnic University, Hung Hom, Kowloon, Hong Kong Special Administrative Region

J.-L. Guyader

Laboratoire Vibrations-Acoustique, INSA Lyon, 25 bis, av. Jean Capelle, 69621 Villeurbanne Cedex, France

A micro-perforated panel (MPP) with a backing cavity is a well known device for efficient noise absorption. This configuration has been thoroughly studied in the experimental conditions of an acoustic tube (Kundt tube), in which the MPP is excited by a normal incident plane wave in one dimension. In a more practical situation, the efficiency of MPP may be influenced by the vibro-acoustic behavior of the surrounding systems as well as excitation. To deal with this problem, a vibro-acoustic formulation based on the patch transfer functions (PTF) approach is proposed to model the behavior of a micro-perforated structure in a complex vibro-acoustic environment. PTF is a substructuring approach, which allows assembling different vibro-acoustic subsystems through coupled surfaces. Upon casting micro-perforations and the flexibility of the MPP under transfer function framework, the proposed PTF formulation provides explicit representation of the coupling between subsystems and facilitates physical interpretation. As an illustration example, application to a MPP with a backing cavity located in an infinite baffle is demonstrated. The proposed PTF formulation is finally validated through comparison with experimental measurements available in the literature. © 2012 Acoustical Society of America. [DOI: 10.1121/1.3682055]

I. INTRODUCTION

Since the pioneer work by Maa,[1] micro-perforated panels (MPP) have been extensively used to design various sound absorption devices. The basic configuration is the one in which an air gap/cavity is placed at the back of the MPP, which creates a Helmholtz sound absorption effect, resulting in effective sound absorption. This basic configuration has been thoroughly studied both theoretically and experimentally using an acoustic tube (Kundt tube) to quantify its absorption ability. In such a situation, the system has one single dimension and the MPP is excited by a normal incident plane wave. The prevailing motivation behind these efforts is the assumption that the acoustic property of the MPP is assumed to be locally reactive. Upon obtaining the surface acoustic impedance or the sound absorption coefficient, the MPP will be treated as conventional sound absorption materials.

Meanwhile, in the pursuit of a more efficient sound absorption, effort has also been made to use MPP in forming a more complex system, which deviates more or less from the basic configuration mentioned previously. Such devices, taking various forms, can loosely be refereed as micro-perforated structure. Double layer[2–4] or multiple layer

absorbers[5] using MPPs are typical examples. The insertion of an additional micro-perforated panel increases the acoustic resistance of the absorber and extends the effective absorption band toward a lower frequency. The performance of the device, however, is limited by the coupling between the MPP and the backing cavity. By transforming the conventional rectangular cavity to an irregular-shaped cavity,[6] the coupling can be modified and manipulated through distortion of the acoustic mode by tilting cavity walls. The change of the cavity geometry promotes more acoustic modes into the coupling and thereby improves the sound absorption performance at selected frequency bands.

Conventionally, MPP was used for building applications. More recently, MPP found its use in more compact mechanical systems in various applications. Typical examples include MRI scanners,[7] acoustic liners in the flow duct[8] or the nacelles of turbofan engines, and interiors of engine enclosures and hoods in tractors, boats, and construction equipment.[9] More specifically, MPP could be used for reducing the engine noise in an automotive passenger compartment. For such applications, it is necessary to evaluate the MPP effect by taking into account the modal behavior of the engine and the passenger compartments, as well as the acoustic and the structural transmissions through the two compartments. Excitations to MPP are then the vibrations and the noise generated by the engine. This is a typical example of what is called the complex vibro-acoustic

a)Author to whom correspondence should be addressed. Electronic mail: mmlcheng@polyu.edu.hk

environment in this paper. This trend of using MPP in these cases in the real industrial setting brings about one critical issue. In fact, most of the existing works focused on a MPP device itself, usually validated in a Kundt tube. When placed in a practical environment, however, experimental methods usually become the only option.[10,11] More importantly, the efficiency of the MPP is shown to be strongly influenced by the vibro-acoustic behavior of the surrounding systems as well as excitations, which are significantly different from the Kundt tube setting.[6,7,9] Therefore, the increasing complexity of the system calls for efficient tools to model and optimize the performance of the MPP in a complex vibro-acoustic environment. Versatility, efficiency, and flexibilities are among the top attributes of the list of major attributes required for such simulation tools, which unfortunately are still lacking in the literature.

This paper attempts to propose a method based on the patch transfer function (PTF) approach to model the MPP behavior in a practical acoustic environment. To illustrate the idea, a general complex vibro-acoustic environment of the MPP is schematically represented in Fig. 1(a). Subject to acoustic or mechanical excitations, the whole system is composed of acoustic cavities, semi-infinite acoustic domain, absorbing materials, and flexible panels, which are coupled through surfaces. PTF (Ref. 12) is a substructuring approach that allows assembling different vibro-acoustic subsystems through coupled surfaces. In the present case, the global system is divided into different subsystems as shown on Fig. 1(b). Each coupling surface connecting a pair of subsystems is further divided into elementary areas called patches. The transfer functions, called patch transfer functions, of each

uncoupled subsystem patch are calculated to form a database. For a mechanical structure, the PTFs are defined as the ratio of the mean velocity over the mean force on a patch, equivalent to patch structural mobilities. For an acoustic domain, the PTFs are defined as the ratio of the mean pressure over the mean velocity on a patch, which are the patch acoustic impedances. Using the superposition principle for linear systems and the continuity relation among different subsystems, the PTF approach allows calculating the response of a global system from the PTFs of uncoupled subsystems by inverting a square symmetric matrix whose dimension corresponds to the number of patches.

The PTFs can be calculated using different methods depending on the subsystem considered. For cavities or flexible structures, these PTFs can be obtained from modal expansions for academic cases or from finite element simulation for complex cases. For semi-infinite acoustic domains, the Rayleigh integral may be used for a plane boundary or boundary element method for a more complex geometry. The sound absorption material may be directly taken into account by its surface impedance. These calculations have been developed and validated for different applications.[12–14] The method, however, has not been used to treat a MPP element, as it cannot be categorized into any of the existing conventional subsystems. It should be noted that, calculations of PTFs are performed beforehand for each subsystem separately. As a result, parallel computation is possible. Moreover, when a finite element method (FEM) is used, the size of the numerical models of each subsystem is considerably smaller than that of the global model. In a typical design problem, re-calculations of PTFs are required only
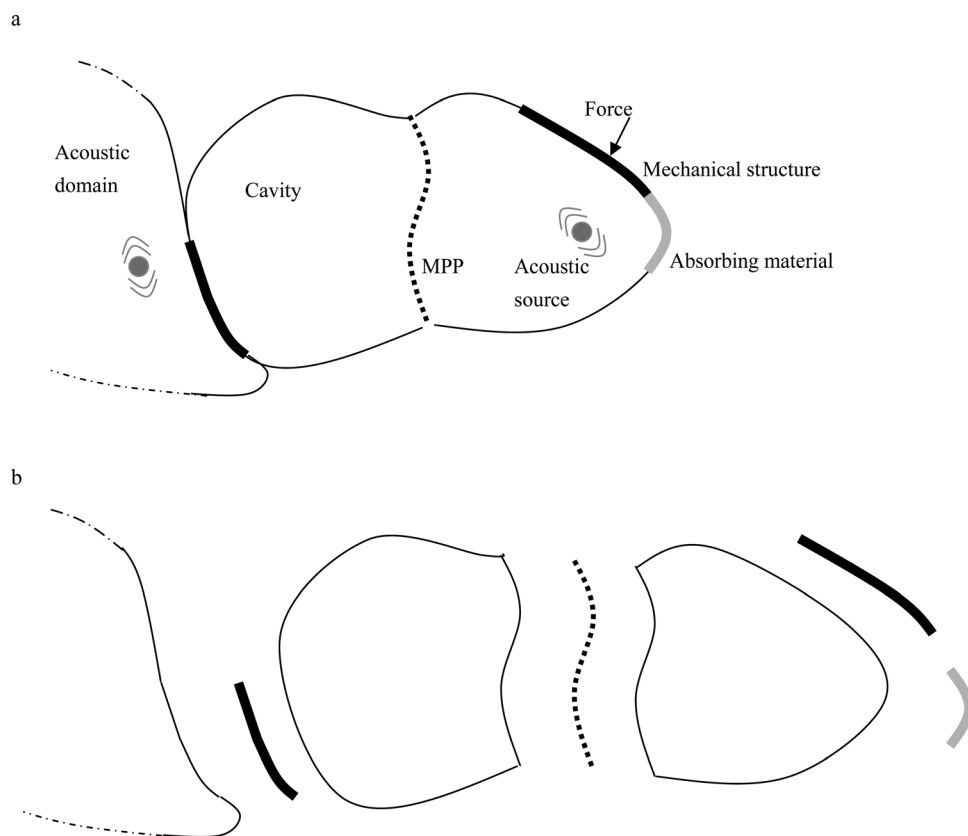

FIG. 1. (a) MPP in a practical vibro-acoustic environment. (b) PTF substructuring.

for those subsystems or components with modifications, endowing the method with the flexibility and efficiency in dealing with complex systems, conducive to conducting system optimization.

In this paper, a new formulation for calculating the PTFs of MPP is first proposed. In a first step, the equations of motion of the MPP are expressed on each patch of the coupling surface. The patch flexural velocity of the MPP and the patch acoustic velocity of the surrounding acoustic medium are then linked to the difference of the patch pressures on both sides of the MPP. Two approaches are then proposed: The first one consists of resolving directly the global problem using the MPP relation as a coupling condition with other subsystems. In this formulation, acoustic and mechanical PTFs of each individual subsystem intervene directly in the global equations. Upon casting micro-perforations and the flexibility of the MPP under the PTF framework, the proposed PTF formulation provides explicit representation of the coupling between subsystems and facilitates an explanation of physical phenomenon. The second approach consists in first calculating the equivalent PTF of a MPP with a backing cavity, which can be further coupled with the PTFs of other acoustic domains in a second step. This second formulation is then explored to illustrate the application of the proposed model to a cavity-backed MPP absorber with an infinite baffle. This allows a deep analysis on the coupling between the MPP and the backing cavity and a quantification of their effects on the sound absorption. It is shown that a MPP with the backing cavity does not behave like a locally reactive material, especially at resonances of the backing cavity. Finally, the proposed model is validated through comparisons with experimental results given in the literature.[15]

II. PRINCIPLE OF PTF APPROACH

Let us consider the basic vibro-acoustic problem presented in Fig. 2, corresponding to a thin elastic structure coupled on both sides with an acoustic domain. The acoustic domain may either be closed or semi-infinite. The PTF approach is briefly recalled here based on this basic system for the sake of clarity, bearing in mind that the methodology can be extended to more complex linear systems.

Assuming harmonic excitations at an angular frequency ω, we are interested in the steady response of the system, omitting the time dependence in the notation. Along the

surface S_c occupied by the thin structure, the whole system is partitioned into three subsystems: An elastic structure and the two acoustic domains at each side. The coupling surface S_c is then divided into N elementary surfaces ∂S_i, $i \in [1, N]$, called patches. The size of the patches should be less than the half-wavelength (i.e., $\lambda/2$) corresponding to the highest frequency of interest, either acoustic or structural, whichever is less.[12,14]

The PTFs are defined for each subsystem, with all quantities being defined with respect to the unit normal vector $\vec{n}$ to the coupling surface S_c. For the structure, a constant normal force $\bar{f}_i^s$ is prescribed on patch i, whereas no force is prescribed on the other patches. The PTFs between the two patches, Y_{ij}^s, is defined as the ratio between the mean normal velocity on patch j and the normal force $\bar{f}_i^s$

$$Y_{ij}^s = \frac{\bar{u}_j^s}{\bar{f}_i^s}, \tag{1}$$

where $\bar{u}_j^s$ is the space-averaged normal velocity on the patch, i.e.,

$$\bar{u}_j^s = \frac{1}{\partial S_j} \int_{\partial S_j} u_j^s dS, \tag{2}$$

The previously defined PTFs are equivalent to structural mobilities of the structure.

For each acoustic domain α ($\alpha = 1,2$), a constant normal velocity $\bar{u}_i^\alpha$ is imposed on patch i with a zero normal velocity on the other patches. The PTFs between excited patch i and receiving patch j, Z_{ij}^α, is defined as

$$Z_{ij}^\alpha = \frac{\bar{f}_j^\alpha}{\bar{u}_i^\alpha}, \tag{3}$$

where $\bar{f}_j^\alpha$ is the resulted force from the acoustic pressure p^α on patch j when patch i vibrates with $\bar{u}_i^\alpha$,

$$\bar{f}_j^\alpha = \int_{\partial S_j} p^\alpha dS. \tag{4}$$

The PTFs as defined correspond to the conventional acoustic impedance. In the previous definitions, the overbar in the notation indicates the mean velocities or the sum of the

Acoustic source

Mechanical force

Structure

Acoustic domain 2

Acoustic domain 1
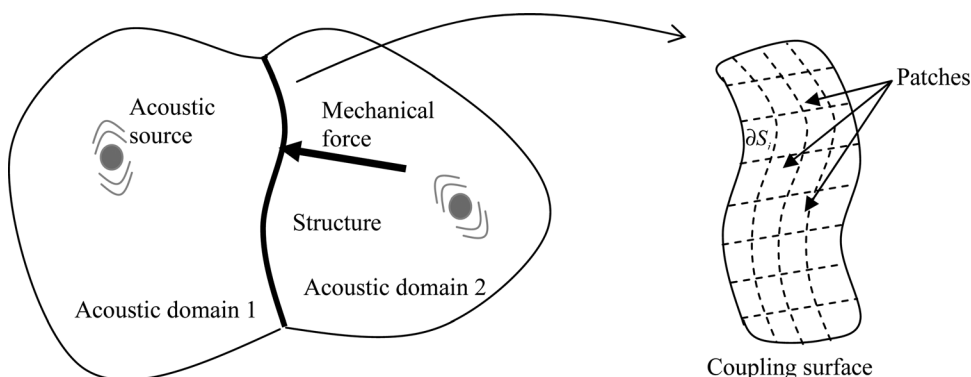
Patches

∂S_i

Coupling surface

FIG. 2. Example of a vibro-acoustic problem.

pressure on the patches [i.e., Eqs. (2) and (4)]. To simplify the notations, these overbars are omitted in the following.

The coupling between the structure and the acoustic domains is performed in two steps.

(1) The first step consists in using the linearity properties of the system to express the relationship between the patch velocities and the patch forces for each subsystem. Indeed, the patch velocity of the structure can be expressed as a sum of the velocity due to the mechanical force acting on the structure before coupling $\tilde{u}_i^s$ and the velocities resulted from the forces exerted on each patch:

$$u_i^s = \tilde{u}_i^s + \sum_{j=1}^{N} Y_{ij}^s f_j^s, \quad \forall i \in [1, ..., N]. \tag{5}$$

Similarly, the force on a patch is equal to the sum of the force corresponding to the acoustic source with a rigid surface, $\tilde{f}_i^\alpha$, and the forces generated by the patch vibrations,

$$f_i^1 = \tilde{f}_i^1 + \sum_{j=1}^{N} Z_{ij}^1 u_j^1, \quad \forall i \in [1, ..., N], \tag{6}$$

$$f_i^2 = \tilde{f}_i^2 + \sum_{j=1}^{N} Z_{ij}^2 u_j^2, \quad \forall i \in [1, ..., N]$$

(2) The second step consists of writing the continuity conditions at each connecting patch, namely the force equilibrium and the equality of normal velocities,

$$u_i^1 = u_i^2 = u_i^s, \quad \forall i \in [1, ..., N], \tag{7}$$

$$f_i^s = f_i^1 - f_i^2, \quad \forall i \in [1, ..., N]$$

where it was assumed that the normal vector is from the acoustic domain 1 toward 2.

Introducing Eqs. (5) and (6) into Eq. (7) yields

$$u_i^1 = \tilde{u}_i^s + \sum_{j=1}^{N} Y_{ij}^s \left(\tilde{f}_j^1 - \tilde{f}_j^2 \right)$$
$$+ \sum_{j=1}^{N} Y_{ij}^s \left[\sum_{k=1}^{N} \left(Z_{jk}^1 - Z_{jk}^2 \right) u_k^1 \right], \quad \forall i \in [1, ..., N]. \tag{8}$$

This system of linear equations with u_i^1 as unknowns may be written in the following matrix form:

$$\mathbf{u}^1 = \tilde{\mathbf{u}}^s + \mathbf{Y}^s \left(\tilde{\mathbf{f}}^1 - \tilde{\mathbf{f}}^2 \right) + \mathbf{Y}^s (\mathbf{Z}^1 - \mathbf{Z}^2) \mathbf{u}^1. \tag{9}$$

Equation (9) is a full system, with its size being equal to the number of patches. Upon resolving this system,

$$\mathbf{u}^1 = \left[\mathbf{I} - \mathbf{Y}^s (\mathbf{Z}^1 - \mathbf{Z}^2) \right]^{-1} \left[\tilde{\mathbf{u}}^s + \mathbf{Y}^s \left(\tilde{\mathbf{f}}^1 - \tilde{\mathbf{f}}^2 \right) \right], \tag{10}$$

where $\mathbf{I}$ is an $N \times N$ identity matrix. All other physical quantities, such as acoustic pressure in each domain can be calculated in a post-processing phase.

The PTF approach allows calculating the response of a global system from the PTFs of uncoupled subsystems by inverting a square symmetrical matrix whose dimension cor-

responds to the number of patches. The PTFs can be calculated by different methods depending on the subsystem considered. These calculations are performed beforehand for each subsystem separately. When FEM is used, the size of the numerical models of each subsystem is considerably smaller than that of the global model. Moreover, the use of incompatible meshes at the subsystem interface is possible, as the problem of compatibility is solved by patch averaging.

III. PTF EQUATIONS FOR THE MICRO-PERFORATED STRUCTURE SUBSYSTEM

Assuming the structure separating the two acoustic domains in Fig. 2 takes the form of a micro-perforated structure, corresponding PTF equations will be developed in the following sections.

A. Modeling of micro-perforated structure

Considering a MPP element shown in Fig. 3, the sound pressure difference between the two sides of MPP, $p^1 - p^2$ generates the vibration of air mass u^0 at each single hole. As the orifice diameter of the hole is much smaller than the acoustic wavelength of interests, it is appropriate to assume that the air particle velocity is distributed uniformly within the area of each hole. Let Z_0 denote the complex acoustic impedance of the hole normalized by the characteristic impedance $\rho_0 c_0$, where ρ_0 is the air density and c_0 the speed of sound. Z_0 is given by[16,17]

$$Z_0 = \frac{32\eta t}{\rho_0 c_0 d^2} \left[\left(1 + \frac{K^2}{32} \right)^{0.5} + \frac{\sqrt{2}}{32} K \frac{d}{t} \right]$$
$$+ i \frac{\omega t}{c_0} \left[1 + \left(1 + \frac{K^2}{32} \right)^{-0.5} + 0.85 \frac{d}{t} \right], \tag{11}$$

where ω is the angular frequency; t is the thickness of the structure; d is the orifice diameter; η is the coefficient of viscosity, and $K = d\sqrt{\omega \rho_0 / 4\eta}$. The real part is the resistive term, which corresponds to the viscous force, whereas the imaginary part is the reactance term corresponding to the inertial force.

Assume that the MPP is flexible and let u^s be its normal velocity. The viscous force depends on the relative velocity of the air in the hole and the structure, $u^0 - u^s$ and the
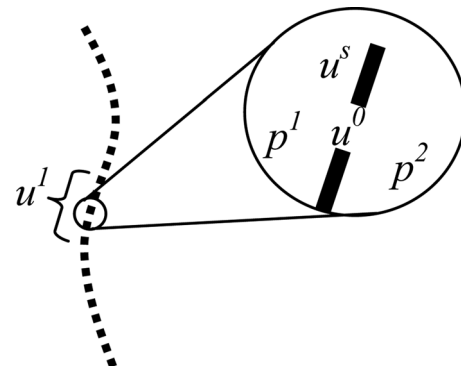

FIG. 3. Description of pressure and velocity variables for the MPP.

J. Acoust. Soc. Am., Vol. 131, No. 3, March 2012

Maxit *et al.*: Micro-perforated panel in complex environment   2121

inertial force depends only on the air velocity. Thus, one can write the following:[17–19]

$$\mathrm{Re}\{Z_0\}(u^0 - u^s) + i\mathrm{Im}\{Z_0\}u^0 = \frac{1}{\rho_0 c_0}(p^1 - p^2). \quad (12)$$

As the orifice diameter of the hole is much smaller than the acoustic and flexural wavelengths of interests, the mean velocity of the surrounding air particle u^1 in the vicinity of the MPP can be approximated from the following relation:

$$u^1 = (1 - \sigma)u^s + \sigma u^0. \quad (13)$$

u^1 allows expressing the velocity continuity conditions of the MPP with the adjacent acoustic domains. On the contrary, u^0 will not be directly used and can be substituted from Eq. (12),

$$u^0 = \frac{1}{\rho_0 c_0 Z_0}(p^1 - p^2) + \frac{\mathrm{Re}\{Z_0\}}{Z_0}u^s. \quad (14)$$

Using the previous expression in Eq. (13) gives

$$u^1 = \left[(1 - \sigma) + \frac{\sigma\mathrm{Re}\{Z_0\}}{Z_0}\right]u^s + \frac{\sigma}{\rho_0 c_0 Z_0}(p^1 - p^2). \quad (15)$$

This relation can be rewritten in a compact form as

$$u^1 = Tu^s + \Psi(p^1 - p^2), \quad (16)$$

where
(i) $T = (1 - \sigma) + \sigma\mathrm{Re}\{Z_0\}/Z_0$ is a non-dimensional parameter that may be called the MPP transmissibility, which represents the contribution of the structural vibrations to the surrounding acoustic particle vibrations and
(ii) $\Psi = \sigma/\rho_0 c_0 Z_0$ is a parameter having m s^{-1} Pa^{-1} as dimension and may be called the equivalent mobility of the perforation.

Equation (16) clearly demonstrates the underlying relationship among the acoustic velocity of the surrounding medium, the pressure difference across the MPP and the vibration of the structure. The resultant velocity in the vicinity of the MPP is a combination of partial transmission of the structural vibration and the air motion of the micro-perforation. The development of the PTF equation for a MPP subsystem in the next section is based on this relation.

B. PTF development

1. Direct formulation

For a MPP patch, as Eqs. (5) and (6) relating the patch pressures and the patch velocities remain valid, the continuity conditions at the connecting patches need to be modified. Indeed, by a space averaging on the patch i of Eq. (16), one has

$$u_i^1 = u_i^2 = Tu_i^s + \Psi(p_i^1 - p_i^2), \quad \forall i \in [1, ..., N]. \quad (17)$$

Meanwhile, the pressure difference $p_i^1 - p_i^2$ acting on the $(1 - \sigma)\partial S_i$ surface of the MPP generates a force, f_i^s, at the patch i,

$$f_i^s = (p_i^1 - p_i^2)(1 - \sigma)\partial S_i, \quad \forall i \in [1, ..., N]. \quad (18)$$

As $f_i^\alpha = p_i^\alpha \partial S_i$, these two relations can be rewritten as

$$u_i^1 = u_i^2 = Tu_i^s + \Psi_i(f_i^1 - f_i^2) \text{ with } \Psi_i = \frac{\Psi}{\partial S_i},$$
$$\forall i \in [1, ..., N]. \quad (19)$$

$$f_i^s = (f_i^1 - f_i^2)(1 - \sigma), \quad \forall i \in [1, ..., N]. \quad (20)$$

The previous expressions describe the continuity conditions in the presence of a micro-perforated structure.

Introducing the linear decompositions Eqs. (5) and (6) into Eqs. (19) and (20), the patch velocity of the acoustic domain 1 can be written as

$$u_i^1 = T\tilde{u}_i^s + \sum_{j=1}^{N}\left(\Psi_i\delta_{ij} + T(1 - \sigma)Y_{ij}^s\right)\left(\tilde{f}_j^1 - \tilde{f}_j^2\right)$$
$$+ \sum_{j=1}^{N}\left[\left(\Psi_i\delta_{ij} + T(1 - \sigma)Y_{ij}^s\right)\sum_{k=1}^{N}\left(Z_{jk}^1 - Z_{jk}^2\right)u_k^1\right],$$
$$\forall i \in [1, ..., N] \quad (21)$$

where δ_{ij} is the Kronecker symbol. The above-mentioned system can be condensed into a matrix form,

$$\mathbf{u}^1 = T\tilde{\mathbf{u}}^s + \left(\boldsymbol{\Psi} + T(1 - \sigma)\mathbf{Y}^s\right)\left(\tilde{\mathbf{f}}^1 - \tilde{\mathbf{f}}^2\right)$$
$$+ \left(\boldsymbol{\Psi} + T(1 - \sigma)\mathbf{Y}^s\right)\left(\mathbf{Z}^1 - \mathbf{Z}^2\right)\mathbf{u}^1, \quad (22)$$

which admits solution in the following form:

$$\mathbf{u}^1 = \left[\mathbf{I} - \left(\boldsymbol{\Psi} + T(1 - \sigma)\mathbf{Y}^s\right)\left(\mathbf{Z}^1 - \mathbf{Z}^2\right)\right]^{-1}$$
$$\times \left[T\tilde{\mathbf{u}}^s + \left(\boldsymbol{\Psi} + T(1 - \sigma)\mathbf{Y}^s\right)\left(\tilde{\mathbf{f}}^1 - \tilde{\mathbf{f}}^2\right)\right]. \quad (23)$$

Note $\boldsymbol{\Psi}$ is a diagonal matrix. In a post-processing phase, the pressure inside the acoustic domains and the velocity on the MPP can be calculated.

Equation (23) seems to differ significantly from Eq. (10). However, if we introduce equivalent PTFs, $\mathbf{Y}^{eq}$ and equivalent free patch velocities, $\tilde{\mathbf{u}}^{eq}$ such that

$$\mathbf{Y}^{eq} = \boldsymbol{\Psi} + T(1 - \sigma)\mathbf{Y}^s, \qquad \tilde{\mathbf{u}}^{eq} = T\tilde{\mathbf{u}}^s, \quad (24)$$

one can rewrite Eq. (23) as

$$\mathbf{u}^1 = \left[\mathbf{I} - \mathbf{Y}^{eq}\left(\mathbf{Z}^1 - \mathbf{Z}^2\right)\right]^{-1}\left[\tilde{\mathbf{u}}^{eq} + \mathbf{Y}^{eq}\left(\tilde{\mathbf{f}}^1 - \tilde{\mathbf{f}}^2\right)\right]. \quad (25)$$

This expression takes the same form as Eq. (10) except that the PTFs and patch free velocities are replaced by their equivalent expressions for the MPP case.

In the case of a rigid MPP (i.e., $\tilde{\mathbf{u}}^s = 0$ and $\mathbf{Y}^s = 0$), Eq. (23) becomes

$$u^1 = \left[I - \Psi(Z^1 - Z^2)\right]^{-1} \Psi\left(\tilde{f}^1 - \tilde{f}^2\right) \qquad (26)$$

and the equivalent PTFs and patch free velocity of the MPP are

$$Y^{eq} = \Psi, \qquad \tilde{u}^{eq} = 0. \qquad (27)$$

Then, the equivalent PTFs are equal to the MPP mobility for the input terms (i.e. $Y^{eq}_{ii} = \Psi_i, \forall i \in [1, ..., N]$) and are null for the cross terms (i.e., $Y^{eq}_{ij} = 0, i \neq j$). In this case, the MPP can be considered as a locally reactive structure characterized by the mobilities Ψ. On the contrary, as can be shown later, a MPP with a backing cavity cannot be considered as a locally reactive device, as opposed to the common assumption made for porous absorbing materials.

2. Equivalent PTFs for a cavity-backed MPP

A typical micro-perforated panel absorber takes the form of a MPP fitted in front of a backing wall or a cavity. The air gap/volume behind the MPP provides an acoustic stiffness,[4] which leads to resonance-type absorption with the perforation. This cavity-backed MPP finds its use in various system configurations and therefore deserves a particular treatment. In order to facilitate the modeling of the overall system involving such devices, a cavity-backed MPP can be regarded as a standalone subsystem. Once the acoustic property is known in terms of PTFs over its surface, it can be integrated into the conventional PTF framework,[12] such providing an alternative to the direct formulation presented in Sec. III B 1. Meanwhile, this will allow a significant simplification and the down-sizing of the number of the subsystems to be handled in a complex system.

To this end, the equivalent PTF of a cavity-backed MPP is defined, to be obtained according to the calculation scheme established hereafter. Consider a typical MPP backed by an acoustic cavity. The outer surface S_c of the cavity-backed MPP is divided into N patches. By imposing a unit normal velocity on patch i, the resulted force on patch j needs to be calculated using the PTFs of the cavity and that of the MPP.

The same matrix notation as in the previous section is used and a Ξ vector is defined as

$$\Xi = [\Xi_k]_{1 \times N}, \qquad \Xi_k = \begin{cases} 1 & \text{for } k = i \\ 0 & \text{otherwise.} \end{cases} \qquad (28)$$

The resulted forces on the patches are contained in the f^1 vector and the imposed velocity condition writes

$$u^1 = \Xi. \qquad (29)$$

The continuity relations (19) and (20) become

$$u^2 = \Xi, \qquad (30)$$

$$Tu^s + \Psi\left(f^1 - f^2\right) = \Xi. \qquad (31)$$

As the MPP and the cavity are not directly excited, Eqs. (5) and (6) become

$$u^s = Y^s f^s, \qquad (32)$$

$$f^2 = Z^2 u^2. \qquad (33)$$

Combining Eqs. (30)–(33) yields

$$\left(\Psi + T(1 - \sigma)Y^s\right)\left(f^1 - Z^2\Xi\right) = \Xi. \qquad (34)$$

The resulting forces f^1 on the patches due to a unit velocity imposed on patch i can be written as follows

$$f^1 = \left[[\Psi I + T(1 - \sigma)Y^s]^{-1} + Z^2\right]\Xi. \qquad (35)$$

This gives the equivalent PTF between patch i and patch j, $\forall j \in [1, N]$. One can finally deduces the equivalent PTF matrix as

$$Z^{eq} = [\Psi I + T(1 - \sigma)Y^s]^{-1} + Z^2. \qquad (36)$$

These equivalent PTFs may be used in the classical PTF approach to characterize the behavior of the MPP with a backing cavity. In such cases, the standard continuity relations Eq. (7) should be used to assemble the equivalent PTFs with the PTFs of the connected subsystem.

Equation (36) also gives indications on the behavior of the system and in particular, on whether the system has a localized reaction. With a rigid MPP, the equivalent PTFs become

$$Z^{eq} = \Psi^{-1} + Z^2 \qquad (37)$$

where Ψ^{-1} is a diagonal matrix. The system is locally reactive if the first term dominates (i.e., $Z^{eq} \approx \Psi^{-1}$). Otherwise, the system is not locally reactive when Z^{eq} is full due to the cavity effect characterized by Z^2. Examples will be given in the next section for a further elaboration of this point.

IV. AN ILLUSTRATION OF APPLICATION

The general framework of a MPP coupled to a complex environment is now established by using the PTF approach. In this section, the proposed method is applied to a basic configuration, which differs from the conventional case of a micro-perforated panel in an acoustic tube. The purpose is to show the potential of the present approach, instead of providing a detailed treatment of the configuration itself.

A. A cavity-backed micro-perforated panel flush-mounted in a rigid baffle

Let us consider a MPP backed by rectangular cavity. The surface of the MPP is flush with a rigid baffle of infinite size. Excited by an incident plane wave $p_0 e^{j[k_0 \sin(\theta)x - k_0 \cos(\theta)z]}$ impinging on the MPP at an angle of incidence θ, the MPP radiates sound toward both the cavity and the semi-infinite acoustic domain. For an easier interpretation of the results, the MPP is supposed to be rigid, bearing in mind that this

assumption is not a limitation of the approach as the structure vibration has already been incorporated into the PTF model. Previous investigations demonstrated that the panel vibration mainly affects the absorption performance at the structural resonances.[19] The size of the panel is 0.5 m × 0.5 m, whereas the depth of the cavity is 0.3 m. The panel thickness, t, and the orifice diameter, d, are both 0.2 mm. The perforation ratio σ is 1%. The acoustic medium is air ($\rho_0 = 1.29$ kg/m^3, $c_0 = 340$ m/s). The first 24 modes of the rigid-walled cavity are tabulated in Table I.

B. PTF calculation procedure

In this section, the MPP backed by a rectangular cavity is flushed with an infinite baffle, the performance of the MPP absorber is thus studied by the PTF method, where three sub-domains, i.e., semi-infinite acoustic medium, MPP, and the cavity, constitute a whole vibro-acoustic system. The coupling surface is divided in 81 patches ($N = 9 \times 9$) ensuring a patch size less than half the acoustic wavelength at 2000 Hz (according to the $\lambda/2$ criteria in Ref. 12). For the semi-infinite domain, the PTFs are estimated by using the Rayleigh integral in Appendix A. It is relevant to note that they are independent of the incident wave and of the characteristics of the MPP.

As the MPP is impinged by an incident plane wave propagating in the semi-infinite medium, the patch blocked forces of the acoustic domain 1, $\tilde{f}_i^1$ are

$$\tilde{f}_i^1 = 2 \int_{\partial S_i} p_{\text{inc}}(M) dS , \quad \forall i \in [1, ..., N], \tag{38}$$

where $p_{\text{inc}}(M) = p_0 e^{j[k_0 \sin(\theta)x - k_0 \cos(\theta)z]}$, and the patch blocked forces of the fluid domain 2 (i.e., cavity), $\tilde{f}_i^2$ are

$$\tilde{f}_i^2 = 0 , \quad \forall i \in [1, ..., N]. \tag{39}$$

For a normal incident wave $\theta = 0°$, one has

$$\tilde{f}_i^1 = 2p_0 \partial S_i, \quad \tilde{f}_i^2 = 0, \quad \forall i \in [1, ..., N] \tag{40}$$

Using these patch blocked forces and the PTFs of the cavity and the semi-infinite medium, one can calculate the patch velocities, u_i^1, $\forall i \in [1, ..., N]$ from Eq. (23) when the MPP is coupled with the backing cavity on one side and the semi-infinite medium on the other side.

The acoustic power absorbed by the cavity-backed MPP, Π_{abs} can then be derived from

$$\Pi_{\text{abs}} = \frac{1}{2} \sum_{i=1}^{N} p_i^1 (u_i^1)^* \partial S_i, \tag{41}$$

where the asterisk denotes the complex conjugate. The patch pressures, p_i^1, can be calculated from

$$p_i^1 = \frac{1}{\partial S_i} \left(\tilde{p}_i^1 + \sum_{j=1}^{N} Z_{ij}^1 u_j^1 \right). \tag{42}$$

The absorption coefficient α_{abs} is defined as the ratio of the absorption power over the incident power through the MPP surface:

$$\alpha_{abs} = \frac{\Pi_{abs}}{\Pi_{inc}}, \tag{43}$$

where Π_{inc} is the acoustic power injected on the MPP surface by the incident plane wave propagating freely in the acoustic medium,

$$\Pi_{\text{inc}} = \frac{1}{2} \frac{p_0^2}{\rho_0 c_0} \sum_{i=1}^{N} \partial S_i. \tag{44}$$

C. Analysis of results

The results shown in this section concern an incident plane wave, normal to the MPP surface and having unit amplitude ($p_0 = 1$ Pa). As can be seen from Sec. IV B, although the oblique incident wave excitation is not a limitation of the current model, we stick to the normal incident case so that results can be compared with literature.

1. Absorption coefficient

The sound absorption coefficient is calculated using the PTF formulation described in Sec. IV B. Numerical results are compared with the results of the equivalent electric circuit method in Fig. 4. Note the electric circuit method considers an infinite MPP with an air gap of the same depth in the one-dimensional case. With a limited panel size, the three-dimensional system considered in the present PTF scheme differs significantly from the classical one-dimensional case. Figure 4 shows that the two methods give similar results in the high frequency range, whereas significant differences occur at low frequencies. At some frequencies, PTF results give a sound absorption coefficient greater than one for our system. This behavior can be explained by the fact that the present system is a three-dimensional one, in

TABLE I. Natural frequencies of the rectangular cavity with rigid boundaries.

$f_{q,r,s}$ (Hz)	0	340	481	567	660	680	743	760	885	948	961	1020
(q,r,s)	0,0,0	0,1,0	1,1,0	0,0,1	0,1,1	0,2,0	1,1,1	1,2,0	0,2,1	1,2,1	2,2,0	0,3,0
		1,0,0			1,0,1	2,0,0		2,1,0	2,0,1	2,1,1		3,0,0
$f_{q,r,s}$ (Hz)	1075	1116	1133	1167	1183	1215	1226	1231	1321	1350	1360	1364
(q,r,s)	1,3,0	2,2,1	0,0,2	0,3,1	0,1,2	1,3,1	2,3,0	1,1,2	0,2,2	2,3,1	0,4,0	1,2,2
	3,1,0			3,0,1	1,0,2	3,1,1	3,2,0		2,0,2	3,2,1	4,0,0	2,1,2

which the "edge effect"[20–24] occurs. In the low frequency range, the diffraction phenomenon in the vicinity of the edge of the MPP results in an increase of the energy absorption coming from the neighborhood of the edges. This can be better seen by investigating the acoustic intensity in the neighborhood of the MPP. The calculation of the acoustic intensity in the framework of the PTF is described in Appendix B. The acoustic intensity maps are then plotted for three selected frequencies corresponding to the local maxima (of Fig. 4) in Fig. 5. One can clearly observe that at 150 Hz, corresponding to the maximum absorption, the energy entry into the MPP comes not only from the front of the MPP due to the acoustic incidence, but also from the side way of the MPP (due to the diffraction effect). As the definition of the absorption coefficient only considers the acoustic power of the incident wave over a surface corresponding to the MPP surface [see Eq. (43)], the acoustic power diffracted from the side of the MPP is not taken into account. This results in an underestimation of the actual power impinging on the panel and an absorption coefficient greater than one in the low frequency range. For higher frequencies, Fig. 5 shows the absorbed power predominately comes from the front and the effect of the diffraction becomes more and more negligible when frequency increases. This can also be reflected in Fig. 4 in which the corresponding sound absorption coefficient is lower than one.

Based on this understanding, one can surmise that the size of the MPP with respect to the acoustic wave length should play an important role in this phenomenon. This was indeed shown in the past by different authors considering classical absorbing material of finite sizes.[15–18] They showed that the absorption coefficient of a patch of absorbent material depends on the size of the patch relative to the wavelength. In general, the absorption coefficient increases when the size of the patch material decreases. The same phenomenon has been observed in the present MPP case, in agreement with the previous studies.[21–24] It should be noted however that these studies considered porous or fibrous absorbing materials, which present rather poor absorption at low frequencies. On the
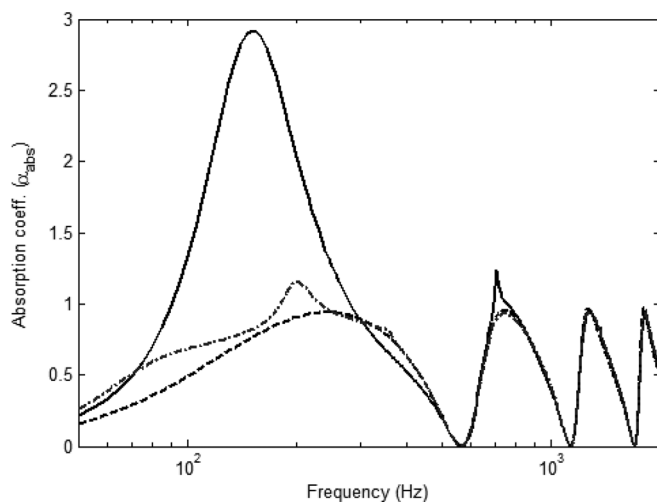
contrary, depending on its design, cavity-backed MPP provides efficient sound absorption even at relatively low frequencies, where the acoustic wavelength is large. By the same token, the size effect is also reinforced in the case of a MPP.
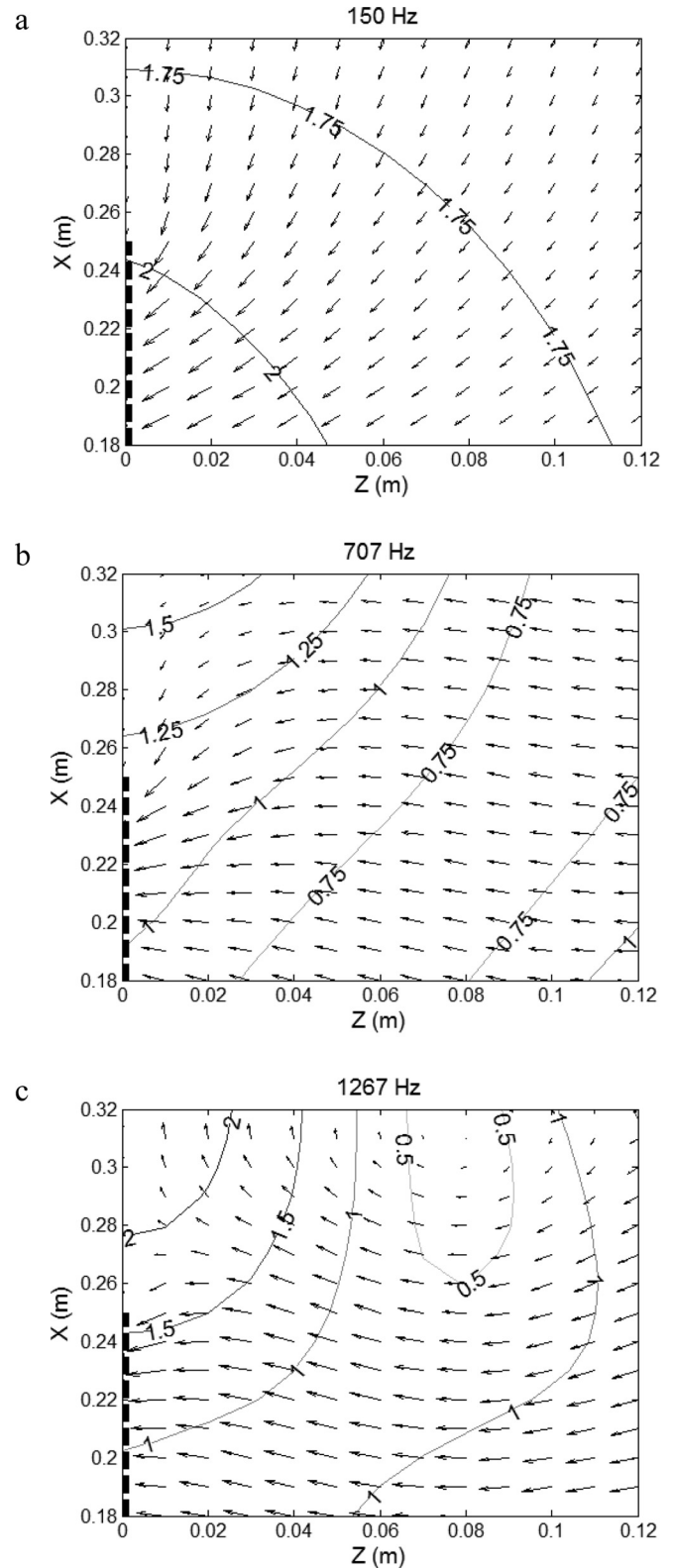

FIG. 5. Acoustic intensity (arrow) and acoustic pressure (contour line) in a plane at $Y = 0.25$ m in the front of the MPP. Normal incidence of the plane wave. MPP position symbolized by a dashed line. (a) 150 Hz, (b) 707 Hz, And (c) 1267 Hz.

FIG. 4. Absorption coefficient versus frequency. Solid line: PTF result for a 0.5 m × 0.5 m MPP; dashed-dotted line: PTF result for a 2 m × 2 m MPP; dashed line: equivalent circuit result.

J. Acoust. Soc. Am., Vol. 131, No. 3, March 2012

Maxit et al.: Micro-perforated panel in complex environment   2125

By increasing the MPP size to 2 m × 2 m, we approach more closely to the infinite panel scenario, which the equivalent circuit method can model. Results obtained form the current PTF approach is superposed to the two existing curves in Fig. 4. It can be seen that using a larger panel, the present PTF approach gives similar result as the equivalent circuit method does, such demonstrating the validity of the approach. Meanwhile, the first sound absorption peak is indeed reduced, in agreement with the previous analysis.

2. Equivalent patch transfer functions

The proposed PTF formulation provides explicit representation of the coupling between subsystems and facilitates interpretation of physical phenomena. This feature is explored using the current system of cavity-backed MPP in terms of the equivalent PTFs defined in Sec. III B 2.

The equivalent PTFs are calculated and depicted in Fig. 6 for three different frequencies. Figure 6(a) shows that at 150 Hz, the equivalent PTF matrix, Z^{eq} [Eq. (37)] is a diagonal-dominant matrix and Z^2 in Eq. (37) is negligible comparing with Ψ^{-1}. This shows that the system is rather locally reactive at this frequency. This gives

$$Z^{eq} \approx \frac{\partial S}{\Psi} I, \tag{47}$$

where ∂S is the surface of the patches. At this frequency, the equivalent PTFs depend only on the equivalent mobility of the perforation Ψ and the surface of the patches, indicating the strong dominance of the MPP. On the contrary, for the two other frequencies corresponding to the first two modes of the hard-walled cavity, the equivalent PTF matrices are full matrices as shown in Figs. 6(b) and 6(c), which implies that the system has not a localized reaction. In this case, the behavior of the cavity-backed MPP is dominated by the cavity. The equivalent PTFs vary in function of the pressure modal variation on the coupling surface. As an extreme example, for the third modes (0,0,1) at 567 Hz, the PTFs are quasi-constant as shown in Fig. 6(c) due to the uniform spatial shape of this mode on the coupling surface. Slight variations at the diagonal terms are due to the term $\partial S/\Psi$ in Eq. (37).

It is pertinent to mention that $\partial S/\Psi$ is the impedance of the perforation and becomes the impedance of the MPP when the vibration of the MPP is neglected. The comparison between this impedance term and the impedance of the cavity provides very useful physical insight in the way the MPP is coupled to the cavity. This is done in Fig. 7, in which the impedance of the MPP, $\partial S/\Psi$, is compared to that of the cavity Z_{ii} for one particular patch (3,4). It can be seen that, $\partial S/\Psi$ are generally larger than Z_{ii}, except for frequencies close to the natural frequencies of the cavity. Provided these modes are excited, the equivalent PTFs correspond to the cavity impedance at their resonance frequencies. In that case, the effect of the MPP becomes negligible compared to the cavity resonance. One such example is the mode (0,0,1) at 567 Hz. As the acoustic damping inside the cavity is small
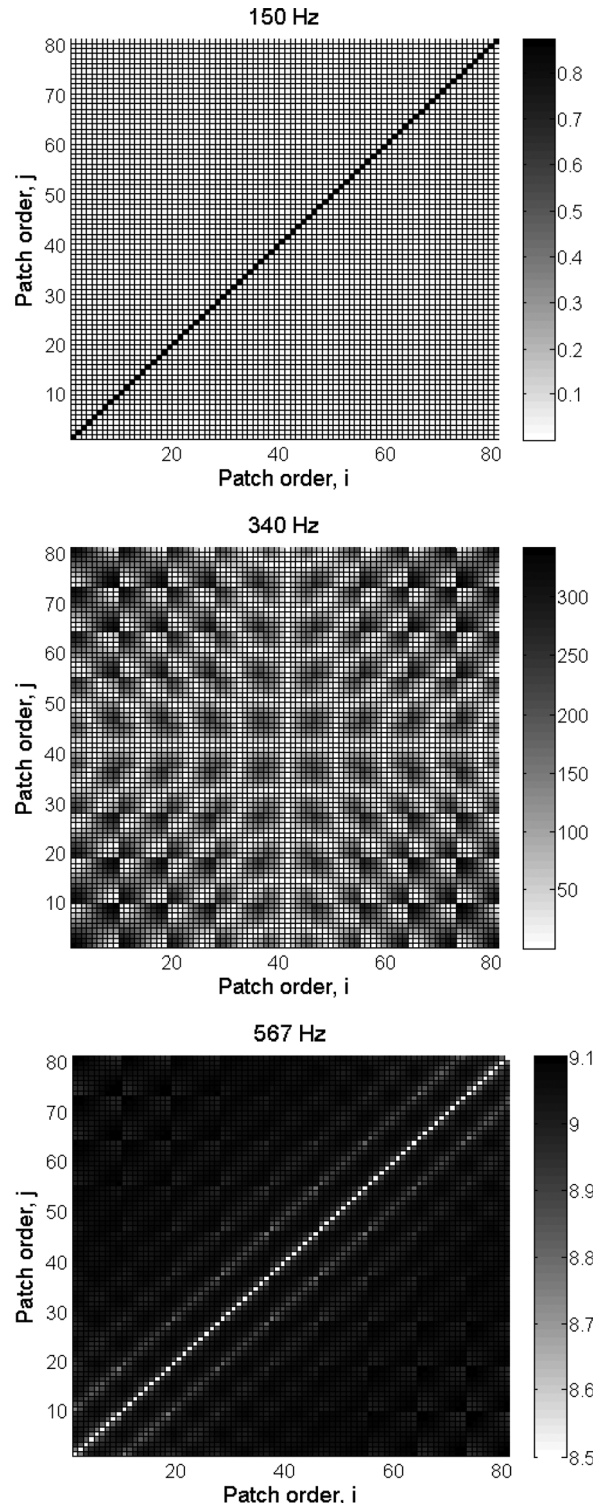

FIG. 6. Magnitude of the equivalent patch transfer functions [N/(m/s)].

($\eta = 0.0001$), the absorption coefficient is quasi-null at this frequency, as shown in Fig. 4. Similar observations can be made at 1133 and 1700 Hz, which correspond to the natural frequencies of modes (0,0,2) and (0,0,3), respectively. It should be mentioned that quite a few acoustic modes cannot be excited due to the nature of the normal incident wave, which are reflected in the sound absorption curve.

In conclusion, the equivalent PTFs of the cavity-backed MPP allows representing the MPP coupled with the backing
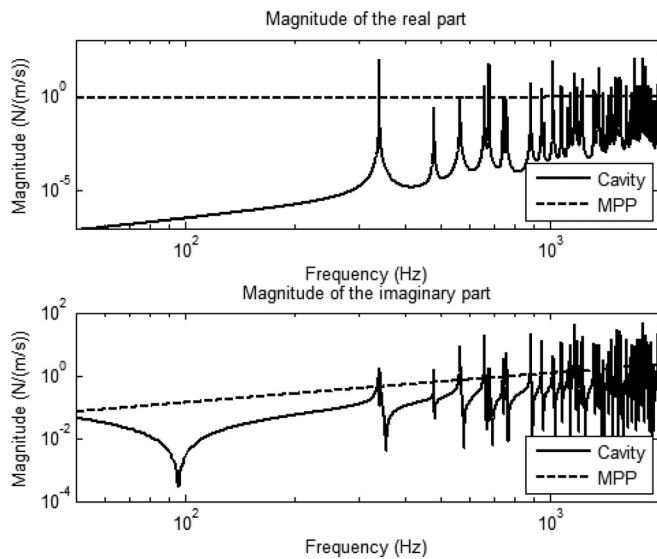
FIG. 7. Comparison of the term $\partial S/\Psi$ of MPP with the PTF of the cavity.

cavity as a single PTF subsystem. In general, this subsystem cannot be considered as a locally reactive material.

V. EXPERIMENTAL VALIDATIONS

The proposed PTF approach is used to investigate the acoustic field inside a rectangular cavity used in Fenech *et al.*[15] Results obtained from the present approach are compared with the experimental data reported in that paper. This comparison allows further validation of the proposed approach in a more complex vibro-acoustic environment. The rectangular air cavity of dimension 2 m × 1.2 m × 0.2 m was made of 22 mm fiberboard panels screwed and glued together. As shown in Fig. 8, a loudspeaker with a diameter of 9 cm was mounted on one of the vertical side panels to provide a white noise excitation to the cavity. The sound pressure was measured at various locations for three configurations: (a) The empty cavity; (b) a MPP installed at the middle of the cavity at $x = 1$ m; and (c) a MPP installed near the cavity wall at $d = 0.25$ m (Fig. 9). In Fenech *et al.*[15] the reverberation time of the empty cavity was found to be ~0.5 s in most of the frequency range of interest. This allows the estimation of an overall damping loss factor from $\eta = 2.2/fT_r$, where f is the frequency and T_r the reverberation time. The aluminum MPP was 1 mm thick and supplied
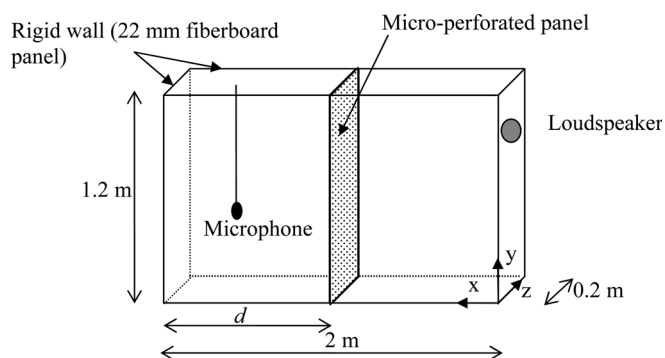

FIG. 8. Rectangular cavity used in the experiments by Fenech *et al.* (Ref. 15).
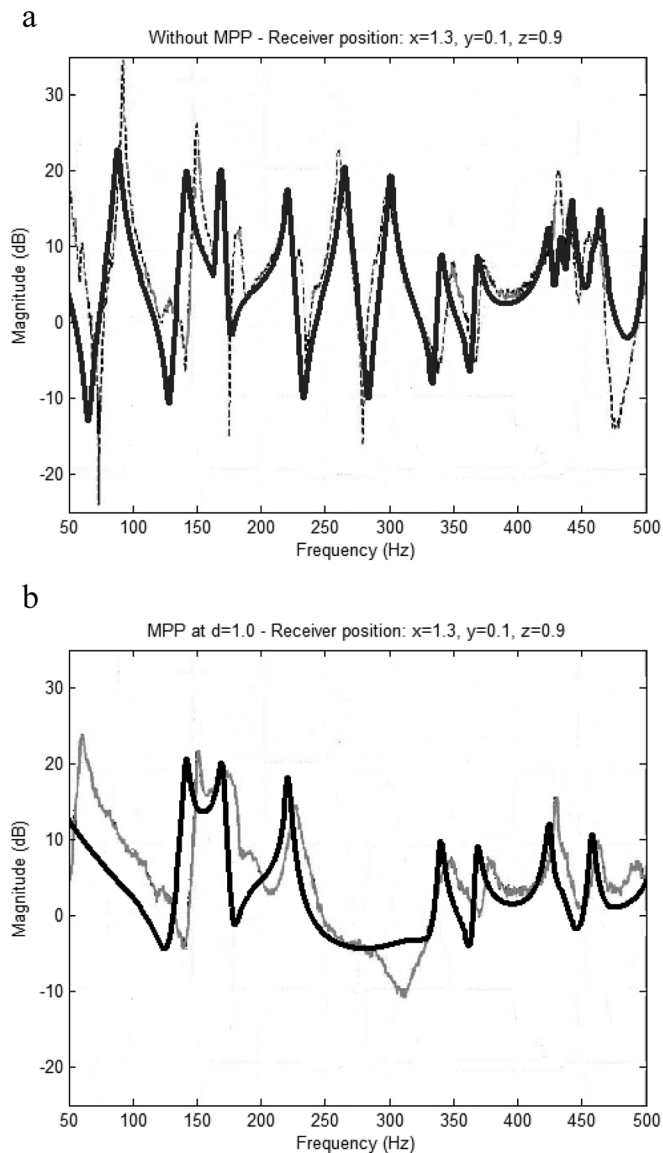

FIG. 9. Comparison of sound pressure calculated by PTF (solid line) with the measurement by Fenech *et al.* (Ref. 15) (gray line) for two cases: (a) Empty cavity and (b) with a MPP at $d = 1.0$ m.

by the Swedish manufacturer Sontech under the trade name Acustimet. Due to the manufacturing process, the punched perforations were found to produce holes with sharp edges that protrude out of the surface of the plate. Therefore, instead of using Maa's theory,[16] the flow impedance Z_0 was experimentally measured using an impedance tube and used in their model.[15] The vibration of the MPP was supposed to be negligible, i.e., $Y_{ij}^s = 0, \forall (i,j) \in [1,N]^2$ in the present formulation.

When the MPP is placed inside the cavity the system is divided into three subsystems: The MPP, and the two rectangular subcavities. The rectangular coupling surface is divided in five patches to ensure the convergence of the solution up to 500 Hz, according to the $\lambda/2$ criterion. The PTFs of the subcavities are calculated from the modal method using rigid-walled modes of the subcavities below 1000 Hz (Appendix A). This calculation is the most time consuming part, even though it requires only few seconds in

J. Acoust. Soc. Am., Vol. 131, No. 3, March 2012

Maxit *et al.*: Micro-perforated panel in complex environment 2127

the present case. These PTFs are also used for calculating the response of the empty cavity in the PTF approach. In this case, the system has only two subsystems, namely the two subcavities, connected by a virtual surface between them at the middle of the cavity. Of course, it is straightforward to use modes of the entire cavity in a modal expansion scheme for estimating the response of the empty cavity. The goal of treating the system by PTF approach is to highlight the efficiency of the method through comparisons with experimental measurement.

Comparisons between the present PTF and experimental results obtained by Fenech *et al.* are given in Fig. 9 in terms of sound pressure level at the measurement point. For the empty cavity, Fig. 9(a) shows a satisfactory agreement between these two sets of results, despite some noticeable differences in the resonance frequencies as well as the peak values. The discrepancy in frequencies may be due to the cavity boundary used in experiment, which does not totally comply with the theoretical model. The frequency shift between the experimental curves and the theoretical ones, in particular in the low frequency, has already been noticed by Fenech *et al.* In their paper. the authors emphasized that the experimental arrangement is not perfect and resulted the frequency shifts due to vibro-acoustic interactions between the sound field inside the cavity and the cavity walls. Indeed, the first non-zero natural frequency of the cavity was predicted at 88 Hz by the present PTF approach, as opposed to 93 Hz measured experimentally and 86 Hz calculated from analytical solutions under the assumption of rigid walls. It is remarkable that, although this frequency does not correspond to any of the natural frequencies of the subcavities, it was correctly predicted using PTF approach.

With the MPP placed at the middle of the cavity, similar comparisons are plotted in Fig. 9(b). Again, the agreement between the PTF results and the experimental results is globally good. Compared with Fig. 9(a), the effect of the MPP can be observed: some resonance frequencies of the empty cavity are altered by the presence of the MPP on one hand, and reduction of some resonance peaks due to the sound absorption of the MPP on the other hand. An attenuation of up to 25 dB for some modes [i.e., (1,0), (3,0), (3,1) noticed in the experiment of Fenech *et al.*] are reproduced by the current model. It is noteworthy that due to the location of the MPP, some modes are practically not affected by the presence of the MPP.

As the last example, Fig. 10 compares the PTF result with that obtained by the calculation by Fenech *et al.*, based on the complex mode evaluation of the modified cavity, along with the experimentally measured sound pressure level when the MPP was placed toward a wall of the cavity at $d = 0.25$ m. Despite some differences, the agreement between the experiment and the simulation is generally satisfactory, bearing in mind that the sound pressure level is sensitive to the location of the measurement point. Similar agreement was also observed for other figures presented in Ref. 15 (not shown here). The two calculation models give very similar results albeit more apparent discrepancies occur at higher frequencies. Differences and uncertainties in the modeling (i.e., damping model, modal convergence) and the data (i.e., damping value, flow impedance value) may explain these differences. Fenech *et al.* have also noticed some discrepancies between the magnitudes of some modes and they have attributed to the fact that the inherent damping of the cavity was measured on one-third octave bands. The introduction of the wooden frame supporting the plate has changed the geometry of the two subcavities and is also a source of uncertainty. In conclusion, these comparisons demonstrate the validity of the present PTF formulation in dealing with systems of various configurations.

VI. CONCLUSIONS

A vibro-acoustic formulation based on the patch transfer functions (PTF) approach is proposed to model microperforated structures in a complex vibro-acoustic environment. The PTFs of the micro-perforated structure is first formulated. Its coupling with surrounding acoustic domains is then cast into a transfer function paradigm through velocity continuity and force equilibrium over connecting patches. This leads to two different formulations, namely direct formulation and equivalent PTFs for cavity-backed micro-perforated structure, both providing explicit representation of the coupling between subsystems and facilitating physical interpretation.

Owing to its substructuring nature, the PTF approach proposed in this paper is an efficient tool to deal with microperforated structure in a complex vibro-acoustic environment. Calculations of PTFs are performed beforehand for each subsystem separately. As a result, parallel computation is possible. In a typical design problem, re-calculations of PTFs are required only for those subsystems or components with modifications, endowing the method with the flexibility and efficiency in dealing with complex systems, conducive to conducting system optimization.

As an illustration example, application to a MPP with a backing cavity located in an infinite baffle is demonstrated. The
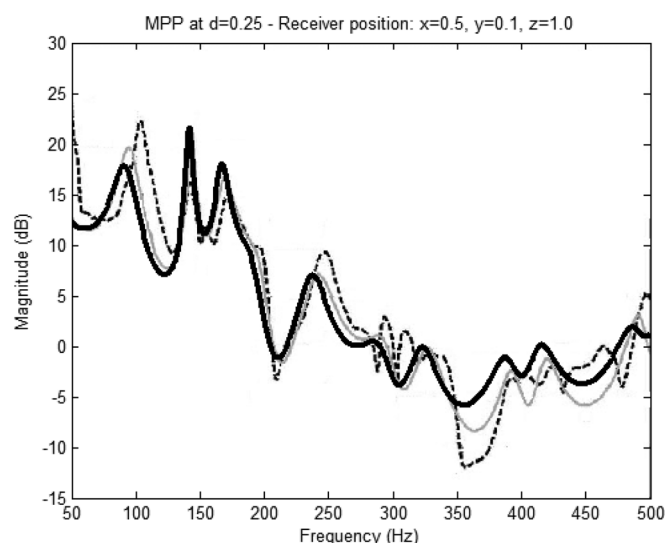

FIG. 10. Comparison of PTF results with the pressures measured and calculated by Fenech *et al.* (Ref. 15) for a MPP at $d = 0.25$ m. Solid line: PTF results; dashed line: Measurement by Fenech *et al.*; and gray line: Prediction by Fenech *et al.*

Maxit *et al.*: Micro-perforated panel in complex environment

proposed PTF formulation is finally validated through comparison with experimental measurements available in the literature.

As a final note, it is relevant to mention that the PTF approach has been applied to several basic systems in this paper. It can be extended to more practical cases with complex geometries. In that case, the patch transfer functions of each subsystem may be calculated by numerical methods like finite element method or boundary element method. The size of the numerical models of each subsystem is considerably smaller than that of the global model.

ACKNOWLEDGMENTS

APPENDIX A: PTFs FOR A SEMI-INFINITE ACOUSTIC DOMAIN

Let us consider a semi-infinite acoustic domain where a unit normal velocity is prescribed on the patch i and where the other patches are supposed to be rigid. The pressure at point M inside or at the boundary of the acoustic domain is given by the following Rayleigh integral equation:

$$p_M = \frac{j\rho_0\omega}{2\pi} \int_{\partial S_i} \frac{e^{-jk_0\|QM\|}}{\|QM\|} dQ, \tag{A1}$$

where $k_0 = \omega/c_0$ is the acoustic wavenumber. Note that the integrand is singular (tends to infinity) as $\|QM\|$ tends to zero. This problem that intervenes in the calculation of the PTF of patch i, Z_{ii} must be overcome by the use of cylindrical coordinates by considering a circular patch having the same surface as the original one (see Ref. 9):

$$Z_{ii} = \rho_0 c_0 \left(1 - e^{-jk_0 a_i}\right) \partial S_i. \tag{A2}$$

For the PTF between patch i and patch j ($i \neq j$), the patch surfaces ∂S_i and ∂S_j are discretized in K and K' elementary surfaces, respectively. As the distance $\|QM\|$ is quasi-constant for Q belonging to an element surface, the integral of Eq. (A1) is approximated by

$$p_M = \frac{j\rho_0\omega\partial S_i}{2\pi K} \sum_{k=1}^{K} \frac{e^{-jk_0\|Q_kM\|}}{\|Q_kM\|}. \tag{A3}$$

where Q_k is the center point of the kth elementary surface.

Thus, the PTF between patch i and patch j can be evaluated by

$$Z_{ij} = \frac{j\rho_0\omega\partial S_i\partial S_j}{2\pi KK'} \sum_{k=1}^{K} \sum_{k'=1}^{K'} \frac{e^{-jk_0\|Q_kQ_{k'}\|}}{\|Q_kQ_{k'}\|}, \tag{A4}$$

and the patch PTF between the patch i and the receiving point M' inside the semi-infinite acoustic medium by

$$Z_{iM'} = \frac{j\rho_0\omega\partial S_i}{2\pi K} \sum_{k=1}^{K} \frac{e^{-jk_0\|Q_kM'\|}}{\|Q_kM'\|}. \tag{A5}$$

APPENDIX B: ACOUSTIC INTENSITY CALCULATION IN A SEMI-INFINITE SPACE WITH PTF FORMALISM

The acoustic intensity at point M' in the direction ς is defined by

$$I_\xi(M') = \frac{1}{2}\text{Re}\left\{p_{M'}^1 u_{\xi,M'}^{1*}\right\}, \tag{B1}$$

where $u_{\xi,M'}^1$ is the acoustic velocity in the ς direction at point M' and the asterisk denotes the complex conjugate.

The pressure at point M' can be calculated from the patch velocities, u_i^1,

$$p_{M'}^1 = \tilde{p}_{M'}^1 + \sum_{i=1}^{N} Z_{iM'}^1 u_i^1, \tag{B2}$$

where the blocked pressure at point M' due to the incident wave is

$$\tilde{p}_{M'}^1 = 2p_0 \cos[k_0\cos(\theta)z]e^{j[k_0\sin(\theta)x]}. \tag{B3}$$

In order to calculate the acoustic velocities at point M' with the same process, one should introduce a supplementary patch transfer function between patch i and point M', $T_{\xi M'}^1$ defined as the acoustic velocity in the c direction at point M' when a normal velocity, $\bar{u}_i^1$ is prescribed on patch i (when other patches are supposed rigid):

$$T_{\xi M'}^1 = \frac{u_{\xi,M'}}{\bar{u}_i^1}, \tag{B4}$$

where $u_{\xi,M'}$ is the acoustic velocity in the ς direction at point M'.

The particle velocity can be related to the pressure gradient using Euler's equation,

$$u_{\xi,M'}^1 = \frac{j}{\rho_0\omega}\frac{\partial p_{M'}^1}{\partial \xi}. \tag{B5}$$

The pressure gradient can be calculated from Eq. (A3) when a unit normal velocity is prescribed on patch i. Finally, one obtains

$$T_{\xi M'}^1 = \frac{\partial S_i}{2\pi K} \sum_{k=1}^{K} \frac{\overrightarrow{Q_kM'}\cdot\vec{\xi}}{\|Q_kM'\|}\left[\frac{jk_0 e^{-jk_0\|Q_kM'\|}}{\|Q_kM'\|} + \frac{e^{-jk_0\|Q_kM'\|}}{\|Q_kM'\|^2}\right]. \tag{B6}$$

Using these PTFs and the patch velocities, u_i^1, the velocity at point M' in the ς direction can be calculated from

$$u_{\xi,M'}^1 = \tilde{u}_{\xi,M'}^1 + \sum_{i=1}^{N} T_{iM'}^1 u_i^1, \tag{B7}$$

where the blocked velocity $\tilde{u}_{\xi,M'}^1$ is determined by

J. Acoust. Soc. Am., Vol. 131, No. 3, March 2012

Maxit *et al.*: Micro-perforated panel in complex environment   2129

$$\tilde{u}_{\xi,M'}^1 = \frac{j}{\rho_0 \omega} \frac{\partial}{\partial \xi} \left\{ 2p_0 \cos[k_0 \cos(\theta)z]e^{j[k_0 \sin(\theta)x]} \right\}. \quad \text{(B8)}$$

Finally, the acoustic intensity at point M' in the direction ς can be obtained by introducing Eqs. (B2) and (B7) in relation (B1).

[1]D. Y. Maa, "Theory and design of microperforated-panel sound-absorbing construction," Sci. Sin. **XVIII**, 55–71 (1975).

[2]Z. M. Zhang and X. T. Gu, "The theoretical and application study on a double layer microperforated sound absorption structure," J. Sound Vib. **215**, 399–405 (1998).

[3]K. Sakagami, K. Matsutani, and M. Morimoto, "Sound absorption of a double-leaf micro-perforated panel with an air-back cavity and a rigid-back wall: Detailed analysis with a Helmholtz–Kirchhoff integral formulation," Appl. Acoust. **71**, 411–417 (2010).

[4]K. Sakagami, T. Nakamori, M. Morimoto, and M. Yairi, "Double-leaf micro-perforated panel space absorbers: A revised theory and detailed analysis," Appl. Acoust. **70**, 703–709 (2009).

[5]D. H. Lee and Y. P. Kwon, "Estimation of the absorption performance of multiple layer perforated panel systems by transfer matrix method," J. Sound Vib. **278**, 847–860 (2004).

[6]C. Q. Wang, L. Cheng, J. Pan, and G. H. Yu, "Sound absorption of a micro-perforated panel backed by an irregular-shaped cavity," J. Acoust. Soc. Am. **127**, 238–246 (2010).

[7]G. Li and C. K. Mechefske, "A comprehensive experimental study of micro-perforated acoustic absorbers in MRI scanners," Magn. Reson. Mater. Phys. **23**, 177–185 (2010).

[8]M. Q. Wu, "Micro-perforated panels for duct silencing," Noise. Control. Eng. J. **45**, 69–77 (1997).

[9]R. Corin and L. Wester, *Sound of Silence* (iVT International, 2005), pp. 105–107.

[10]J. Kang and H. V. Fuchs, "Feasibility of applying microperforated absorbers in acoustic window system," Appl. Acoust. **66**, 669–689 (2005).

[11]H. Droltleff and X. Zhou, "Attractive room acoustics design for multipurpose halls," Acustica. **87**, 500–504 (2001).

[12]M. Ouisse, L. Maxit, C. Cacciolati, and J. Guyader, "Patch transfer functions: a tool to couple linear acoustic problems," J Vibr. Acoust. **127**, 458–466 (2005).

[13]L. Maxit, C. Cacciolati, and J. Guyader, "Airborne noise prediction using patch acoustic impedance," *Proceedings of International Congress on Sound and Vibration ICSV9*, Orlando, FL (2002).

[14]J. Chazot and J. Guyader, "Prediction of transmission loss of double panels with a patch-mobility method," J. Acoust. Soc. Am. **121**, 267–278 (2007).

[15]B. Fenech, G. M. Keith, and F. Jacobsen, "The use of microperforated plates to attenuate cavity resonances," J. Acoust. Soc. Am. **120**, 1851–1858 (2006).

[16]D. Y. Maa, "Potential of microperforated panel absorber," J. Acoust. Soc. Am. **104**, 2861–2866 (1998).

[17]D. Takahaski and M. Tanaka, "Flexural vibration of perforated plates and porous elastic materials under acoustic loading," J. Acoust. Soc. Am. **112**, 1456–1463 (2002).

[18]M. Toyoda, R. L. Mu, and D. Takahashi, "Relationship between Helmholtz-resonance absorption and panel-type absorption in finite flexible microperforated-panel absorbers," Appl. Acoust. **71**, 315–320 (2010).

[19]Y. Y. Lee, E. W. M. Lee, and C. F. Ng, "Sound absorption of a finite flexible micro-perforated panel backed by an air cavity," J. Sound Vib. **287**, 227–243 (2005).

[20]P. E. Sabine, "What is measured in sound absorption measurements," J. Acoust. Soc. Am. **6**, 239–245 (1935).

[21]J. R. Pellam, "Sound diffraction and absorption by a strip of absorbing material," J. Acoust. Soc. Am. **11**, 396–400 (1940).

[22]R. K. Cook, "Absorption of sound by patches of absorbent materials," J. Acoust. Soc. Am. **29**, 324–329 (1957).

[23]J. R. Pellam and R. H. Bolt, "The absorption of sound by small areas of absorbing material," J. Acoust. Soc. Am. **12**, 24–30 (1940).

[24]E. D. Daniel, "On the dependence of absorption coefficients upon the area of the absorbent material," J. Acoust. Soc. Am. **35**, 571–573 (1963).